UvA-DARE (Digital Academic Repository)

University of Amsterdam

Evidence for γ-ray emission from the remnant of Kepler's supernova based on deep H.E.S.S. observations

H.E.S.S. Collaboration; Aharonian, F.; Prokhorov, D.A.; Simoni, R.; Vink, J.

Link to publication

Astronomy & Astrophysics

Evidence for γ-ray emission from the remnant of Kepler's supernova based on deep H.E.S.S. observations[*]

H.E.S.S. Collaboration: F. Aharonian[1,2,3], F. Ait Benkhali[4], E. O. Angüner[5], H. Ashkar[6], M. Backes[7,8],
V. Barbosa Martins[9], R. Batzofin[10], Y. Becherini[11,12], D. Berge[9], K. Bernlöhr[2], M. Böttcher[8], C. Boisson[13],
J. Bolmont[14], M. de Bony de Lavergne[15], M. Breuhaus[2], R. Brose[1], F. Brun[16], T. Bulik[17], T. Bylund[12], F. Cangemi[14],
S. Caroff[14], S. Casanova[18], M. Cerruti[11], T. Chand[8], A. Chen[10], O. Chibueze[8], G. Cotter[19], P. Cristofari[13],
J. Damascene Mbarubucyeye[9], J. Devin[20], A. Djannati-Ataï[11], A. Dmytriiev[13], K. Egberts[21], S. Einecke[22],
J.-P. Ernenwein[5], K. Feijen[22], A. Fiasson[15], G. Fichet de Clairfontaine[13], G. Fontaine[6], S. Funk[23], S. Gabici[11],
Y. A. Gallant[24], S. Ghafourizadeh[4], G. Giavitto[9], L. Giunti[11,16], D. Glawion[23], J. F. Glicenstein[16], M.-H. Grondin[20],
M. Hörbe[19], W. Hofmann[2], T. L. Holch[9], M. Holler[25], D. Horns[26], Z. Huang[2], M. Jamrozy[27], V. Joshi[23],
I. Jung-Richardt[23], E. Kasai[7], K. Katarzyński[28], U. Katz[23], B. Khélifi[11], W. Kluźniak[29], N. Komin[10], K. Kosack[16],
D. Kostunin[9], A. Lemière[11], M. Lemoine-Goumard[20], J.-P. Lenain[14], F. Leuschner[30], T. Lohse[31], A. Luashvili[13],
I. Lypova[4], J. Mackey[1], D. Malyshev[30], V. Marandon[2], P. Marchegiani[10], A. Marcowith[24], G. Martí-Devesa[25],
R. Marx[4], G. Maurin[15], P. J. Meintjes[32], M. Meyer[26], A. Mitchell[23,2], R. Moderski[29], L. Mohrmann[2], A. Montanari[16],
E. Moulin[16], J. Muller[6], K. Nakashima[23], M. de Naurois[6], A. Nayerhoda[18], J. Niemiec[18], A. Priyana Noel[27],
P. O'Brien[33], S. Ohm[9], L. Olivera-Nieto[2], E. de Ona Wilhelmi[9], M. Ostrowski[27], S. Panny[25], M. Panter[2],
R. D. Parsons[31], G. Peron[2], V. Poireau[15], D. A. Prokhorov[34,**], G. Pühlhofer[30], M. Punch[11,12], A. Quirrenbach[4],
P. Reichherzer[16], A. Reimer[25], O. Reimer[25], M. Renaud[24], B. Reville[2], F. Rieger[2], G. Rowell[22], B. Rudak[29],
H. Rueda Ricarte[16], V. Sahakian[35], S. Sailer[2], H. Salzmann[30], D. A. Sanchez[15], A. Santangelo[30], M. Sasaki[23],
J. Schäfer[23], F. Schüssler[16], H. M. Schutte[8], U. Schwanke[31], J. N. S. Shapopi[7], R. Simoni[34,**], H. Sol[13],
A. Specovius[23], S. Spencer[19], Ł. Stawarz[27], S. Steinmassl[2], C. Steppa[21], I. Sushch[8], T. Takahashi[36], T. Tanaka[37],
A. M. Taylor[9], R. Terrier[11], M. Tsirou[2], Y. Uchiyama[38], T. Unbehaun[23], C. van Eldik[23], J. Veh[23], J. Vink[34,**],
H. J. Völk[2], S. J. Wagner[4], F. Werner[2], R. White[2], A. Wierzcholska[18], Y. W. Wong[23], A. Yusafzai[23], M. Zacharias[13,8],
D. Zargaryan[1,3], A. A. Zdziarski[29], A. Zech[13], S. J. Zhu[9],
S. Zouari[11], and N. Żywucka[8]

(Affiliations can be found after the references)

ABSTRACT

Observations with imaging atmospheric Cherenkov telescopes (IACTs) have enhanced our knowledge of nearby supernova (SN) remnants with ages younger than 500 yr by establishing Cassiopeia A and the remnant of Tycho's SN as very-high-energy (VHE) γ-ray sources. The remnant of Kepler's SN, which is the product of the most recent naked-eye SN in our Galaxy, is comparable in age to the other two, but is significantly more distant. If the γ-ray luminosities of the remnants of Tycho's and Kepler's SNe are similar, then the latter is expected to be one of the faintest γ-ray sources within reach of the current generation IACT arrays. Here we report evidence at a statistical level of 4.6σ for a VHE signal from the remnant of Kepler's SN based on deep observations by the High Energy Stereoscopic System (H.E.S.S.) with an exposure of 152 h. The measured integral flux above an energy of 226 GeV is ~0.3% of the flux of the Crab Nebula. The spectral energy distribution (SED) reveals a γ-ray emitting component connecting the VHE emission observed with H.E.S.S. to the emission observed at GeV energies with *Fermi*-LAT. The overall SED is similar to that of the remnant of Tycho's SN, possibly indicating the same nonthermal emission processes acting in both these young remnants of thermonuclear SNe.

Key words. gamma rays: general – supernovae: individual: Kepler – ISM: supernova remnants – radiation mechanisms: non-thermal

1. Introduction

For several decades, supernova remnants (SNRs) have been considered the most likely sources of Galactic cosmic rays (CRs; e.g., Ginzburg & Syrovatskii 1964), that is, CRs with energies at least up to 3×10^{15} eV. While the detection of radio and X-ray synchrotron radiation from SNRs does indeed prove that electrons are accelerated to GeV or even of order 10 TeV energies (e.g., Reynolds 2008; Helder et al. 2012; Dubner & Giacani 2015; Vink 2020, for reviews), further insight into the particle acceleration in SNRs comes from γ-ray astronomy, which inter alia provides a probe of CR protons and nuclei through observations of GeV to TeV emission resulting from the decay of secondary neutral pions produced in CR interactions.

Over the last two decades, SNRs have been established as an important population of Galactic γ-ray sources, both in the high-energy (HE) domain (100 MeV to 100 GeV) by the *Fermi* Large Area Telescope (LAT) observations (Acero et al. 2016) and in the very-high-energy (VHE) domain (>100 GeV) by observations with imaging atmospheric Cherenkov telescopes (IACTs); an SNR population study is provided in H.E.S.S. Collaboration (2018a) and an overview of VHE γ-ray astrophysics in Hinton & Hofmann (2009).

Very-high-energy spectra by themselves are often insufficient to firmly establish whether the γ-ray emission is produced by accelerated protons and other atomic nuclei (so-called CR hadrons) or by accelerated electrons (CR leptons), or both. However, in some cases the presence of a characteristic pion-decay feature in the sub-GeV part of the γ-ray spectrum (the "pion-decay bump") can clearly establish a hadronic origin for the γ-ray emission. This is for example the case for SNRs IC 433 and W44 (Ackermann et al. 2013). In other cases, due to the fact that CR hadrons lead to a softer γ-ray spectrum (with a photon index of $\Gamma = 2.0$ for a hadron power-law index of 2) in the HE regime than CR leptons ($\Gamma = 1.5$ in the Thomson regime for a lepton power-law index of 2), the spectral shape can indicate the production mechanism of the emission. However, a correspondence between spectral slopes and origin of γ-ray emission can be more complex if gas clumps are present (Gabici & Aharonian 2014) or in the case of nonlinear diffuse shock acceleration (Malkov 1999), as well as for leptonic emission in the Klein-Nishina regime (Porter et al. 2006).

Supernova remnants with ages younger than 2000–3000 yr have been established as TeV γ-ray sources. This fact suggests that CRs are accelerated to >10 TeV when the shock velocities are still in excess of a few thousand km s^{-1} (Helder et al. 2012). Many of these young TeV γ-ray emitting SNRs belong to the class of historical SNRs, that is, SNRs produced by naked-eye supernovae (SNe) recorded in history, such as SN 185/RCW 86 (H.E.S.S. Collaboration 2018b), SN 1006 (Acero et al. 2010), and SN 1572 (also known as Tycho's SNR; Archambault et al. 2017). The young SNRs, RX J1713.7−3946 (H.E.S.S. Collaboration 2018c) and particularly Cassiopeia A (Cas A; Ahnen et al. 2017; Abeysekara et al. 2020), which are the possible remnant of SN 393 (Wang et al. 1997) and the remnant of a nearby 340-year-old SN missing in records, respectively, are also sometimes added to this SNR class. With these additions, both remnants of core-collapse SNe (RX J1713.7−3946 and Cas A) and thermonuclear (Type Ia) SNe (SN 185, SN 1006, and SN 1572/Tycho's SNR) are included. Based on the γ-ray spectral characteristics, the γ-ray emission from Tycho's SNR and Cas A are likely of hadronic origin (Morlino & Caprioli 2012; Ahnen et al. 2017; Abeysekara et al. 2020), whereas for the other, more extended, 1000- to 3000-year-old SNRs a leptonic origin (for RX J0852.0−4622; see Aharonian et al. 2005; Lee et al. 2013; H.E.S.S. Collaboration 2018d) has been suggested. However, a hadronic scenario for these older TeV γ-ray emitters has also been discussed, for example in Berezhko et al. (2012), Inoue et al. (2012), and Gabici & Aharonian (2014).

The remnant of the youngest naked-eye SN of AD 1604 (also known as Kepler's SNR; Green & Stephenson 2017; Vink 2017), is conspicuously absent from the above list of young SNRs detected in VHE γ rays. Kepler's SNR is, however, a known X-ray synchrotron emitter (Allen et al. 1999; Nagayoshi et al. 2021), indicating that particles, at least electrons, are accelerated up to ~10 TeV. Moreover, the relatively high density of its ambient medium (e.g., Williams et al. 2012) makes Kepler's

SNR a probable candidate for being a γ-ray source dominated by hadronic emission. The High Energy Stereoscopic System (H.E.S.S.) experiment observed Kepler's SNR in the past, but the previous observations did not result in a detection of the remnant (Aharonian et al. 2008). This is partially due to the relatively short exposure time (13 h) compared to other SNRs, as well as the fact that Kepler's SNR, located at about 5 kpc (Ruiz-Lapuente 2017), is more distant than the historical SNRs listed above.

At GeV energies, an excess at about a 4σ statistical level from Kepler's SNR was reported by Xiang & Jiang (2021) and in the proceedings by Prokhorov et al. (2021). In Xiang & Jiang (2021), the authors claimed a detection of γ-ray emission from Kepler's SNR despite the presence of residual radiation around Kepler's SNR and concluded that more observation data with IACTs and *Fermi*-LAT are necessary to firmly confirm the association between the γ-ray source candidate and Kepler's SNR. Using a summed likelihood analysis and a larger allowed range of zenith angles, Acero et al. (2022) confirmed a detection of Kepler's SNR above a 6σ level based on 12 yr of *Fermi*-LAT data.

In this paper, we present the results of deep observations of Kepler's SNR performed with H.E.S.S. for a total of 152 h. This data set is significantly larger than the data comprising 13 h of observations used in the previous publication (Aharonian et al. 2008). We report first evidence for VHE γ-ray emission from Kepler's SNR – the last remaining historical SNR that had until now escaped detection at these energies. Combining the H.E.S.S. VHE data with HE data from 10.7 yr of *Fermi*-LAT observations, we explore models to interpret the broad γ-ray spectral energy distribution (SED), in terms of hadronic and leptonic emission processes.

2. Observations and analysis

In this section, we present data reduction and analyses of H.E.S.S. and *Fermi*-LAT data (Sects. 2.1.1 and 2.2.1), and results obtained from these analyses (Sects. 2.1.2 and 2.2.2).

2.1. H.E.S.S. telescopes

The H.E.S.S. experiment is a hybrid array of five IACTs located in the southern hemisphere in Namibia (23°16′18″ S, 16°30′00″ E) at an altitude of ~1800 m above sea level (Aharonian et al. 2006). The H.E.S.S. array consists of four 12 m diameter telescopes (Ashton et al. 2020) placed in a square with 120 m sides and one 28 m diameter telescope in the center of the array. A 28 m diameter telescope installed in 2012 complements the array, but is not used in this analysis. Detection of VHE γ rays with the four 12 m telescopes is based on the stereoscopic reconstruction technique. We performed the dedicated observations of Kepler's SNR with H.E.S.S. reported in this paper using wobble mode with pointing offsets of 0°7 in right ascension or declination from Kepler's SNR, allowing a simultaneous measurement of the background in the same field of view (Berge et al. 2007).

2.1.1. Data reduction and analysis

We took data with at least three participating telescopes and in 28 min exposures called runs. We used the standard data quality selection procedure to identify observations with satisfactory hardware states of the instrument and good atmospheric
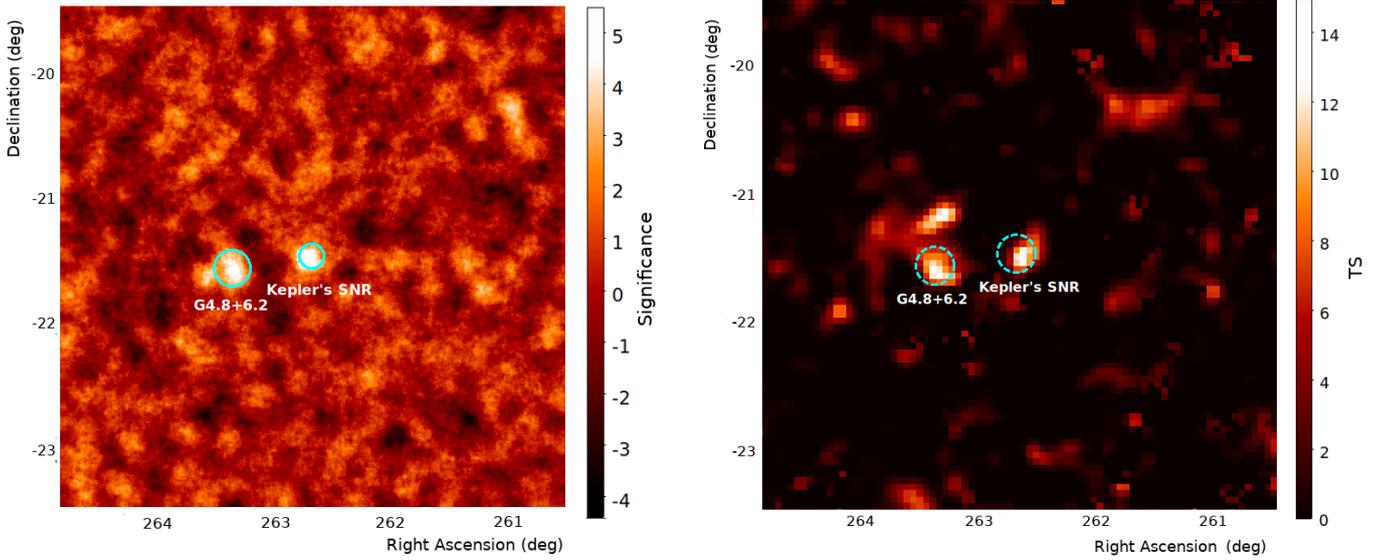
Fig. 1. H.E.S.S. and *Fermi*-LAT maps. *Left panel*: H.E.S.S. γ-ray significance map of Kepler's SNR using an oversampling radius of 0°.1. *Right panel*: *Fermi*-LAT TS map in the range of 4.75−300 GeV. The position of Kepler's SNR is in the center of these maps. Solid circles in the left panel correspond to the source regions of Kepler's SNR and SNR G4.8+6.2 (to the east of Kepler's SNR), while dashed circles in the right panel merely indicate the locations of these SNRs. Neither of these sources are present in the 4FGL catalog.

conditions ([Aharonian et al. 2006](#)). We analyzed 152.2 h of good-quality data recorded during 353 runs. Of these, 122 h were accumulated in 2017−2020, whereas the remaining 30 h were spread over the years 2004−2013. The mean zenith angle of these observations is 26°. Given the age of Kepler's SNR, we assume its VHE γ-ray emission to be steady during the time interval of 16 yr (4% of the age of Kepler's SNR) in which the H.E.S.S. observations took place. This permits a simultaneous spectral fit of both the *Fermi*-LAT and H.E.S.S. data.

We analyzed the H.E.S.S. data using the `Model Analysis` ([de Naurois & Rolland 2009](#)) and used an analysis configuration that requires a minimum of 60 photo-electrons per image and considers events with an estimated direction reconstruction uncertainty of less than 0°.1. We cross-checked the results with the `Image Pixel-wise fit for Atmospheric Cherenkov Telescope (ImPACT)` analysis ([Parsons & Hinton 2014](#)). We defined a circular region-of-interest with a radius of 6′ around the geometrical center of Kepler's SNR (at RA = $17^h30^m40.8^s$, Dec = $-21°29'11''$) – hereafter referred to as the source region. This radius corresponds to the selection cut for a VHE point-like source. Kepler's SNR with 3.5′ diameter can be considered as a point-like source for H.E.S.S. enclosed within the source region.

2.1.2. VHE γ-ray results

The data analysis yields 1524 γ-ray-like events from the source region and 23667 γ-ray-like events from a large ring-shaped background (off-source) region, from which we excluded the region with a 0°.3 radius around another potential VHE γ-ray source (SNR G4.8+6.2; see Appendix A). The ratio of the on-source exposure to the off-source exposure, α, is 0.0569. We computed the number of excess counts by subtracting the number of off-source events multiplied by α from the number of events coming from the source region. The γ-ray excess is 178 counts above the background, which corresponds to a significance of 4.6σ according to Eq. (17) from [Li & Ma (1983)](#). The H.E.S.S. significance map is shown in the left panel of Fig. 1. The main and cross-check analyses used in this paper provide compatible results.

We derived the energy spectrum using a reflected region background method ([Berge et al. 2007](#)) and a forward-folding technique ([Piron et al. 2001](#)). The analysis energy threshold for this data set is 226 GeV given by the energy at which the effective area falls to 15% of its maximum value. The likelihood maximization yields a photon index of $\Gamma = 2.3 \pm 0.2_{stat} \pm 0.2_{syst}$ and a normalization constant of $N_0 = (9.5 \pm 2.3_{stat} \pm 2.9_{sys}) \times 10^{-14}\,cm^{-2}\,s^{-1}\,TeV^{-1}$ at $E_0 = 1\,TeV$ for a power-law spectrum $dN/dE = N_0(E/E_0)^{-\Gamma}$. We binned the spectrum in such a way that spectral points require a minimum significance level of 2.0σ each. The derived SED in the energy range from 226 GeV to 19 TeV is shown in Fig. 2. The derived VHE flux is lower by a factor of 2.2 than the 99% flux upper limit reported in the previous publication. The systematic uncertainties are conservatively estimated to be ±0.2 on the photon index and ±30% on the normalization coefficient ([Aharonian et al. 2006](#)).

In addition to the VHE excess at the position of Kepler's SNR, Fig. 1 shows the presence of a hotspot at the position of SNR G4.8+6.2 (see Appendix A), which is ≈0°.7 to the east of Kepler's SNR. The analysis of this hotspot yields a γ-ray excess of 185 counts above the background. The numbers of on- and off-source events are $N_{ON} = 2007$ and $N_{OFF} = 35049$, respectively, with a background-normalization factor $\alpha = 0.0520$. This γ-ray excess is significant at a level of 4.2σ.

2.2. *Fermi*-LAT

The principal instrument on board the *Fermi* Gamma Ray Space Telescope is the Large Area Telescope (LAT; [Atwood et al. 2009](#)), a pair-conversion telescope covering the energy range from about 20 MeV to more than 300 GeV. *Fermi*-LAT has been scanning the entire sky continuously since August 2008.

2.2.1. Data reduction and analysis

As part of the motivation and preparation for the H.E.S.S. observations in 2020, we performed and took into account the analysis of *Fermi*-LAT HE γ-ray data presented in this section. The presence of γ-ray excesses both in H.E.S.S. and *Fermi*-LAT
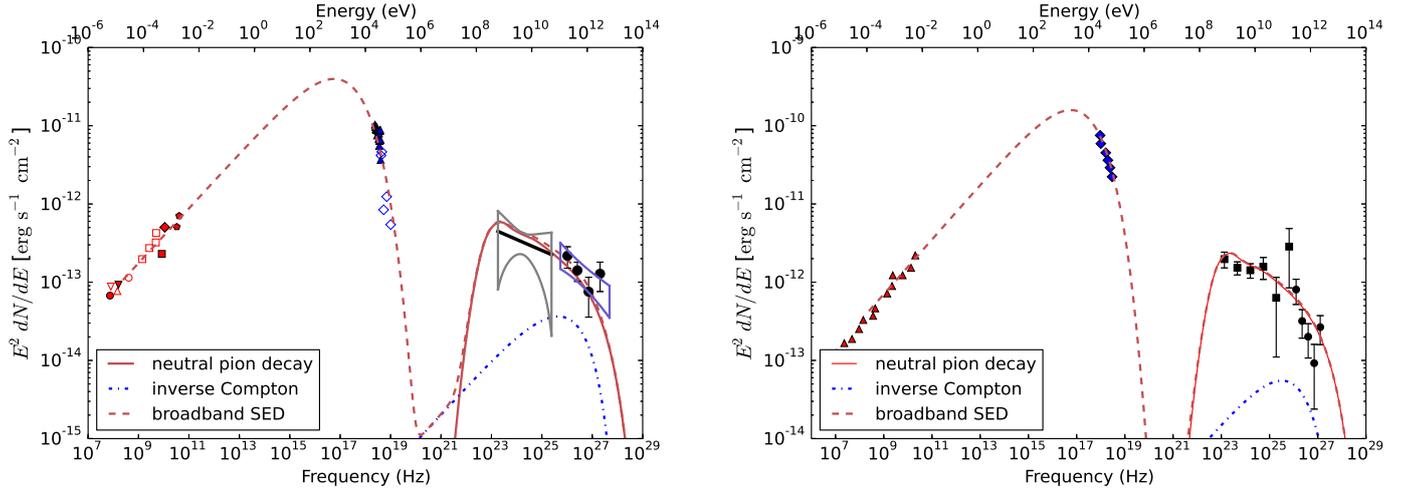
Fig. 2. Broadband SEDs of Kepler's SNR (*left*) and Tycho's SNR (*right*) with hadronic model fits. SED data points and butterfly plots for Kepler's SNR as derived from H.E.S.S. and *Fermi*-LAT data are shown. Observations of Kepler's SNR from the radio band to the X-ray band are from VLA (red filled ○), Culgoora (red ▽), PAPER (red △), Molonglo (red ○), Parkes (red □), NRAO (red ◇), WMAP (red ○), RXTE (blue △), and *Swift*-BAT (blue ◇).

lends credence to the association between these γ-ray signals and Kepler's SNR.

For the data analysis, we used the `Fermitools` v1.2.23 package[1] and P8R3_SOURCE_V2 instrument response functions. We selected *Fermi*-LAT γ-ray events with reconstructed energies between 750 MeV and 300 GeV and performed a binned analysis by choosing a $10° \times 10°$ square region centered at RA = $17^h30^m48.7^s$, Dec = $-20°1'55''$ (region of interest, ROI). We shifted the position of the ROI center from that of Kepler SNR by $1°.4$ in declination to reduce systematic effects due to the presence of a molecular cloud, the Pipe Nebula, and the Galactic plane in the ROI and their contributions to the foreground emission. For this analysis, we selected events accumulated from 2008 August 4 to 2019 May 16. To reduce the contamination by the γ-ray emission from the Earth's limb, we selected events with zenith angles $<90°$. We applied standard quality cuts (`DATA_QUAL>0 && LAT_CONFIG==1`).

To model the sources within the ROI, we included sources from the 4FGL catalog (Abdollahi et al. 2020) within a region of $17°.5$ radius around the center of the ROI. To model the Galactic and isotropic background diffuse emission, we used the standard templates `gll_iem_v07.fits` and `iso_P8R3_SOURCE_V2_v1.txt`. The point spread function of *Fermi*-LAT is sufficiently wide that Kepler's SNR can be treated as a point source. We applied the binned likelihood analysis on the data by using the `Fermitools` routine, `gtlike`. We binned the data in 25 logarithmically spaced bands in energy and used the spatial binning with a pixel size of $0°.1$. We allowed the power-law normalization and photon index of Kepler's SNR and the normalizations of the Galactic and isotropic diffuse sources to vary. We also allowed the normalizations of 4FGL γ-ray sources within $3°$ of Kepler's SNR to vary, while keeping the normalizations of other 4FGL sources fixed. We evaluated the significance of model components or additional parameters using the test statistic, TS = $2(\log \mathcal{L} - \log \mathcal{L}_0)$, where $\mathcal{L}_0$ is the likelihood of the reference model without the additional parameters or components (Mattox et al. 1996).

[1] https://fermi.gsfc.nasa.gov/ssc/data/analysis/software/

2.2.2. HE γ-ray results

For the 0.75–300 GeV energy interval, the derived TS value for Kepler's SNR is 16.8, which corresponds to about 4σ significance. The likelihood maximization yields a photon index of $\Gamma = 2.1 \pm 0.3$ and a normalization constant, $N_0 = (9.3 \pm 3.1) \times 10^{-15}$ cm^{-2} s^{-1} MeV^{-1} at $E_0 = 4750$ MeV for a power-law spectrum. Figure 1 shows the TS map, based on a source model including 4FGL sources plus diffuse backgrounds, generated for the energy range of 4.75–300 GeV for the sake of comparison with the VHE γ-ray results. It reveals similarities between the *Fermi*-LAT TS map and the H.E.S.S. significance map at VHE energies. The positive TS values and significances for Kepler's SNR and SNR G4.8+6.2 are present on both these maps in Fig. 1. The butterfly shaped area shown in Figs. 2 and 3 corresponds to the 68% statistical uncertainty region of the differential flux. The excesses both in *Fermi*-LAT and H.E.S.S. data provide strong support for the identification of Kepler's SNR in the HE and VHE γ-ray bands. Between 0.75 and 300 GeV, the residual emission at the position of SNR G4.8+6.2 is significant at a 3.3σ statistical level (TS = 10.9).

3. Interpretation and modeling

3.1. Young SNRs as γ-ray sources

The hadronic scenario–in which the γ-ray emission is produced through the two-photon decay of neutral pions created in hadron collisions of CRs with background gas–results in viable models for both the Tycho's and Cas A SNRs (Zhang et al. 2013; Ahnen et al. 2017). The leptonic scenario, in which inverse Compton (IC) mechanism dominates the VHE emission, is still a viable scenario for Tycho's SNR under the assumption that its GeV γ-ray emission is due to hadronic interactions (Yuan et al. 2012) or in the two-zone approach (Atoyan & Dermer 2012). However, more recently developed physical models suggest that the γ-ray emission is primarily due to hadronic processes (Morlino & Caprioli 2012; Slane et al. 2014). Tycho's and Cas A SNRs are comparable in age with Kepler's SNR, which allows the radiative properties of SNRs to be investigated at an early stage in their evolution.
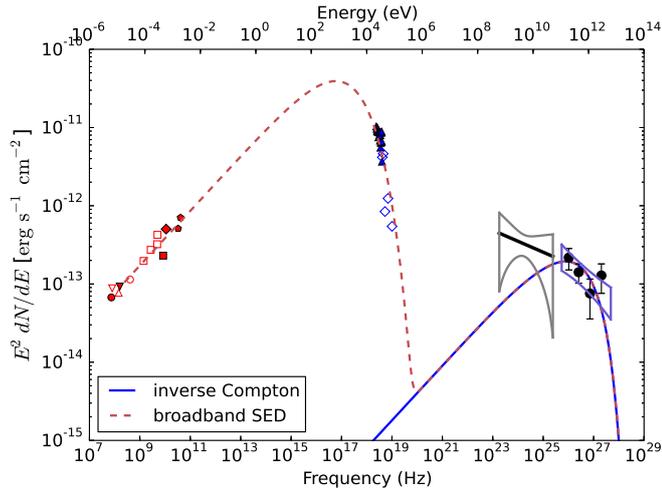
Fig. 3. Broadband SED of Kepler's SNR with a leptonic model fit corresponding to the magnetic field of 80 μG.

Both Type Ia and core-collapse SNe deliver similar kinetic energies of ~10^{51} erg. However, the type of SN does matter for both the ejected mass and the density and structure of the ambient medium. It is conceivable that the TeV emission detected from the Cas A SNR, which resulted from a core-collapse explosion, originates dominantly from the reverse shock instead of from the region heated by the forward shock (e.g., Helder & Vink 2008; Telezhinsky et al. 2013; Zirakashvili et al. 2014). The reverse shock accelerates particles of the ejecta, which, in turn, collide with the metal-rich plasma of the SN ejecta, leading to strong hadronic emission due to the high ejecta density in core-collapse SNRs. This circumstance might hinder a direct comparison of the radiation model for the Cas A SNR with the radiation models for Tycho's and Kepler's SNRs, for which the γ-ray emission is thought to be dominated by forward-shock accelerated particles. The Galactic CR chemical composition, meanwhile, conforms better to acceleration of a well-mixed interstellar medium than metal-rich ejecta (Ellison et al. 1997). For thermonuclear SNe, more time is necessary for the progenitor system to evolve (e.g., Totani et al. 2008); this extra time allows it to wander a long distance away from the parent molecular cloud. Thus, the environment in which the remnants of thermonuclear SNe evolve can be significantly different from the environment of core-collapse SNe of massive stars.

Multiwavelength studies of Kepler's SNR (Vink 2017, for a review) have established that SN 1604 was a Type Ia SN. At a likely distance of 5 kpc (Sankrit et al. 2016; Vink 2017; Ruiz-Lapuente 2017), given the Galactic latitude of 6°.8, Kepler's SNR is located 590 pc above the Galactic plane. The relatively high density around Kepler's SNR, in particular in the northwestern part of the SNR, is attributed to mass lost by the progenitor system (Bandiera 1987; Chiotellis et al. 2012; Williams et al. 2012; Burkey et al. 2013; Toledo-Roy et al. 2014). Apart from its relatively large distance and high Galactic latitude, Kepler's SNR is best compared to Tycho's SNR located at a distance of about 2.5 kpc: both are Type Ia SNRs of similar age and develop in a relatively dense ambient medium with $n \approx 1-10 \, \mathrm{cm}^{-3}$.

3.2. SED models

A variety of multiwavelength data is available for Kepler's SNR. It allows us to construct a characteristic SED for the nonthermal

radiation caused by accelerated particles. In addition to the γ-ray data points described above, we use radio and X-ray spectral data points of Kepler's SNR from Reynolds & Ellison (1992), Allen et al. (1999) along with the WMAP data points at 33 and 41 GHz from Massardi et al. (2009) and the *Swift*-BAT data points at (4.2, 4.5, 5.3, 7.0, and 10.0) × 10^{18} Hz from Oh et al. (2018). For comparison with the SED of Tycho's SNR, the data points in the radio and X-ray bands are from Zhang et al. (2013, and references therein), and the *Fermi*-LAT and VERITAS γ-ray data points are from Archambault et al. (2017). The properties of Kepler's and Tycho's SNRs are described in the Appendix B.

In the framework of a hadronic model, we chose typical numerical values for physical parameters and described both SEDs of Kepler's and Tycho's SNRs by using the modeling package, Naima (Zabalza 2015). The radio band to X-ray band SEDs are attributed to the synchrotron radiation of a CR electron population, while the broad γ-ray SED is attributed to radiation driven by the collisions of relativistic CR protons with gas. Our model setup includes: (i) $E_{SN} = 10^{51}$ erg for the SN Ia explosion energy; (ii) the distances to Kepler's and Tycho's SNRs of 5.0 kpc (Ruiz-Lapuente 2017) and 2.5 kpc (Zhang et al. 2013; Kozlova & Blinnikov 2018), respectively; (iii) $n = 1 \, \mathrm{cm}^{-3}$ for the gas target particle density; (iv) the kinetic energy of CR hadrons above 1 GeV of $E_{CR}/E_{SN} = 7\%$ of the SN Ia explosion energy; (v) $B = 200$ μG for the magnetic field strength[2] (Völk et al. 2005; Helder et al. 2012); (vi) the ratio of energy in CR electrons to that in CR hadrons is 0.5%, constrained by fitting the synchrotron SED component; (vii) $q = 2.3$ for the CR electron and proton spectral indices, $dN_{p,e}/dE \propto E^{-q}$, assumed to be the same and chosen to provide us with a fit in the radio-frequency band (DeLaney et al. 2002; Kothes et al. 2006); and (viii) exponential cut-off energies in the CR proton spectrum at 100 TeV and in the CR electron spectrum at 7.5 TeV, respectively. We assumed a fraction of the SN explosion energy converted into the energy of CRs similar to that given by Berezhko et al. (2006) (that is 10%). The parameter values (iii), (vi), and (viii) are chosen such that the hadronic model matches the SEDs of Kepler's and Tycho's SNRs. The constraint on the proton exponential cut-off energy is however premature, since the power-law hypothesis is currently sufficient to describe the observed SED in the VHE band. We note that the model is sensitive to the combination $E_{CR} \times n$ rather than these two parameters individually. A model-dependent constraint on the density can be set by the size of the SNR at its given age during the adiabatic (Sedov) stage (e.g., Berezhko et al. 2006).

The left and right panels in Fig. 2 show the broadband SEDs of Kepler's and Tycho's SNRs, respectively, along with the hadronic model described above. The observations support the similarity between the shapes of their broadband SEDs. In the framework of this model, the hadronic γ-ray component dominates over the γ-ray component produced by CR electrons.

A comparison of the results presented in Fig. 2 shows that the same hadronic model scaled according to the different distances to the two SNRs describes both the SEDs of Kepler's and Tycho's SNRs. This conclusion supports that these remnants, similar in at least SN type and age, have also similar broadband nonthermal emission properties. The luminosities of Tycho's and Kepler's SNRs at 1 TeV are similar for the assumed distances, whereas the TeV luminosity of Cas A is five times higher. However, the TeV luminosity depends on several parameters, such as

---

[2] The arbitrary value of 200 μG is chosen so as to suppress the IC-to-synchrotron emission ratio and to remain within reasonable downstream magnetic field ranges for these remnants.

the CR energy in the source and the average density. So there is a possibility that the similarity of Tycho's and Kepler's SNR may hide some underlying differences in these parameters. This SED model can also describe the SEDs of Kepler's and Tycho's SNRs even if they are located at 7 kpc and 3.5 kpc, respectively, keeping the same distance ratio as above (that is $5/2.5 = 2$), but increasing the gas density from $1\,\mathrm{cm}^{-3}$ to $(7/5)^2 \times 1\,\mathrm{cm}^{-3} = 2\,\mathrm{cm}^{-3}$. The gas density around Kepler's SNR has a strong gradient, with the southeastern part being more tenuous than the northwestern part. Moreover, the gas appears to be clumpy. Hence, gas densities vary from $n \sim 1$–$250\,\mathrm{cm}^{-3}$ (Williams et al. 2012), and the average gas density is not well constrained. The distribution of γ-ray emission from different gas accumulations in these remnants remains hidden in the model. In future works on modeling, questions to be addressed are the implementation of a gas density distribution, the efficiency of conversion of kinetic energy to HE particles, the cutoff shape in the electron spectrum, and the connection to the dynamical evolution of the SNRs. Future γ-ray studies of Kepler's SNR are required for precise determination of its spectral and morphological characteristics in the VHE γ-ray band and further examination of this joint interpretation.

In a leptonic scenario, the γ-ray emission is produced via IC scattering of photons from the cosmic microwave background (CMB), the infrared photon field emitted by dust in SNRs, and the Galactic interstellar radiation field by energetic electrons. To compute the IC γ-ray component, we included these three photon fields making similar contributions and took energy densities and spectra of the latter two photon fields from Gomez et al. (2012) and Porter et al. (2006). Since the same electron population is emitting both X-rays via the synchrotron mechanism and the HE and VHE γ rays via the IC mechanism, we constrain the magnetic-field strength by requiring that the model reproduces the observed flux of X-ray emission and does not overshoot the H.E.S.S. SED data points. In case the γ-ray emission is dominated by hadronic processes, this constraint should be regarded as a lower limit to the magnetic-field strength (Aharonian et al. 2008). From the γ-ray observations reported above, it follows that for magnetic field values greater than $80\,\mu\mathrm{G}$ the resulting IC flux would be less than the measured γ-ray flux.

Figure 3 illustrates the leptonic model with a magnetic field strength of $80\,\mu\mathrm{G}$. This magnetic-field strength is marginally below than the measured downstream magnetic field strength value for Kepler's SNR, which is in the range of 100–$200\,\mu\mathrm{G}$ (Völk et al. 2005; Helder et al. 2012). The photon index measured from the *Fermi*-LAT data, $\Gamma = 2.1 \pm 0.3$, is softer than that expected for the leptonic scenario, $\Gamma = 1.7$. In order to better determine which emission scenario is preferred, we compared the two models using the likelihood ratio test based on the *Fermi*-LAT data with energies between 750 MeV and 300 GeV. The null model assumes emission via IC scattering with a γ-ray spectrum fit to the H.E.S.S. data. Between 750 MeV and 300 GeV, the γ-ray spectrum in the null model is well approximated by a power law with fixed parameters. The alternative model assumes a power-law model with a free flux normalization and a free photon index, and the best-fit spectral parameters in this model better correspond to the hadronic scenario. The likelihood analysis described in Sect. 2.2 gives the TS value 5.1 with 2 degrees of freedom for a comparison of the null and alternative models. Therefore, the spectral shape favors a hadronic model over a leptonic model with a 1.8σ significance. Acero et al. (2022) have recently performed an analysis of 12 yr of the *Fermi*-LAT data, selecting γ rays above 100 MeV. The derived photon index value is in agreement with that reported above and their lowest energy flux point provides

further support for a hadronic model. The SED at γ-ray energies can also be explained by a mixed scenario involving both leptonic and hadronic contributions.

4. Summary and conclusions

γ-ray observations of young SNRs provide insights into the particle acceleration mechanisms and HE emission processes. HE and VHE γ-ray observations of the Tycho and Cas A SNRs show that remnants younger than 500 yr old emit γ rays likely via the decay of neutral pions created in proton-proton collisions. Sharing a number of the physical properties with Tycho's SNR, Kepler's SNR is an important testbed for a connection between CRs and SNRs.

This paper reports the results of 152 h of VHE observations of Kepler's SNR with H.E.S.S. and provides a characterization of the whole data set using advanced analysis methods. This data set is significantly larger than that used in the previous publication. VHE γ-ray emission from Kepler's SNR is significant at a 4.6σ statistical level. A spectral analysis of this data set yields a photon index of $\Gamma = 2.3 \pm 0.2_{\mathrm{stat}} \pm 0.2_{\mathrm{sys}}$ and a normalization constant of $N_0 = (9.5 \pm 2.3_{\mathrm{stat}} \pm 2.9_{\mathrm{sys}}) \times 10^{-13}\,\mathrm{cm}^{-2}\,\mathrm{s}^{-1}\,\mathrm{TeV}^{-1}$ at $E_0 = 1\,\mathrm{TeV}$. This paper also includes an analysis of 10.7 yr of *Fermi*-LAT data performed before making the decision on H.E.S.S. observations of Kepler's SNR in 2020. This analysis provides an indication of a GeV counterpart of Kepler's SNR and confirms the results reported by Xiang & Jiang (2021) and Acero et al. (2022). The compatibility of the signals in the HE and VHE γ-ray bands supports their common origin and association with Kepler's SNR.

Although the detection at the 4.6σ level falls short of the gold-standard in the field of VHE γ-ray astronomy of $>5\sigma$, our results are based on observations targeting Kepler's SNR directly, and not a blind search. Moreover, Kepler's SNR, being a young SNR and an X-ray synchrotron source, is a priori expected to be a VHE γ-ray source. These arguments altogether provide a strong reason to endorse Kepler's SNR as a faint HE and VHE γ-ray source.

The results show that the observed SED of Kepler's SNR is similar to that of Tycho's SNR, possibly indicating the same non-thermal emission processes acting in both these SNRs. This fact allows us for the first time to tentatively propose a model of γ-ray emission that describes both the SEDs of Kepler's and Tycho's SNRs. It assumes a hadronic origin of the observed γ-ray emission and requires (1) $\approx 10\%$ of the SN Ia explosion energy to be converted to CR hadron energy and (2) the gas target particle density of $\approx 1\,\mathrm{cm}^{-3}$. A lower limit on the magnetic field strength of $B > 80\,\mu\mathrm{G}$ derived from the requirement that the IC γ-ray component does not overshoot the H.E.S.S. SED data points is tighter than the previous lower limit (Aharonian et al. 2008) by a factor of ≈ 1.5.

References

Abdollahi, S., Acero, F., Ackermann, M., et al. 2020, ApJS, 247, 33
Abeysekara, A. U., Archer, A., Benbow, W., et al. 2020, ApJ, 894, 51
Acero, F., Aharonian, F., Akhperjanian, A. G., et al. 2010, A&A, 516, A62
Acero, F., Ackermann, M., Ajello, M., et al. 2016, ApJS, 224, 8
Acero, F., Lemoine-Goumard, M., & Ballet, J. 2022, A&A, 660, A129
Ackermann, M., Ajello, M., Allafort, A., et al. 2013, Science, 339, 807
Aharonian, F., Akhperjanian, A. G., Bazer-Bachi, A. R., et al. 2005, A&A, 437, L7
Aharonian, F., Akhperjanian, A. G., Bazer-Bachi, A. R., et al. 2006, A&A, 457, 899
Aharonian, F., Akhperjanian, A. G., Barres de Almeida, U., et al. 2008, A&A, 488, 219
Ahnen, M. L., Ansoldi, S., Antonelli, L. A., et al. 2017, MNRAS, 472, 2956
Allen, G. E., Gotthelf, E. V., & Petre, R. 1999, Int. Cosm. Ray Conf., 3, 480
Archambault, S., Archer, A., Benbow, W., et al. 2017, ApJ, 836, 23
Ashton, T., Backes, M., Balzer, A., et al. 2020, Astropart. Phys., 118, 102425
Atoyan, A., & Dermer, C. D. 2012, ApJ, 749, L26
Atwood, W. B., Abdo, A. A., Ackermann, M., et al. 2009, ApJ, 697, 1071
Badenes, C., Bravo, E., Borkowski, K. J., & Domínguez, I. 2003, ApJ, 593, 358
Bandiera, R. 1987, ApJ, 319, 885
Bedin, L. R., Ruiz-Lapuente, P., González Hernández, J. I., et al. 2014, MNRAS, 439, 354
Berezhko, E. G., Ksenofontov, L. T., & Völk, H. J. 2006, A&A, 452, 217
Berezhko, E. G., Ksenofontov, L. T., & Völk, H. J. 2012, ApJ, 759, 12
Berge, D., Funk, S., & Hinton, J. 2007, A&A, 466, 1219
Burkey, M. T., Reynolds, S. P., Borkowski, K. J., & Blondin, J. M. 2013, ApJ, 764, 63
Chiotellis, A., Schure, K. M., & Vink, J. 2012, A&A, 537, A139
Coffin, S. C., Williams, B. J., & Katsuda, S. 2022, ApJ, 926, 84
de Naurois, M., & Rolland, L. 2009, Astropart. Phys., 32, 231
DeLaney, T., Koralesky, B., Rudnick, L., & Dickel, J. R. 2002, ApJ, 580, 914
Dubner, G., & Giacani, E. 2015, A&ARv, 23, 3
Duncan, A. R., Stewart, R. T., Haynes, R. F., & Jones, K. L. 1997, MNRAS, 287, 722
Ellison, D. C., Drury, L. O., & Meyer, J.-P. 1997, ApJ, 487, 197
Gabici, S., & Aharonian, F. A. 2014, MNRAS, 445, L70
Gamezo, V. N., Khokhlov, A. M., & Oran, E. S. 2005, ApJ, 623, 337
Ginzburg, V. L., & Syrovatskii, S. I. 1964, The Origin of Cosmic Rays (New York: Macmillan)
Gomez, H. L., Clark, C. J. R., Nozawa, T., et al. 2012, MNRAS, 420, 3557
Green, D. A., & Stephenson, F. R. 2017, in Possible and Suggested Historical Supernovae in the Galaxy, eds. A. W. Alsabti, & P. Murdin, 179
Helder, E. A., & Vink, J. 2008, ApJ, 686, 1094
Helder, E. A., Vink, J., Bykov, A. M., et al. 2012, Space Sci. Rev., 173, 369
H.E.S.S. Collaboration (Abdalla, H., et al.) 2018a, A&A, 612, A3
H.E.S.S. Collaboration (Abramowski, A., et al.) 2018b, A&A, 612, A4
H.E.S.S. Collaboration (Abdalla, H., et al.) 2018c, A&A, 612, A6
H.E.S.S. Collaboration (Abdalla, H., et al.) 2018d, A&A, 612, A7
Hinton, J. A., & Hofmann, W. 2009, ARA&A, 47, 523
Hughes, J. P. 2000, ApJ, 545, L53
Hwang, U., Hughes, J. P., & Petre, R. 1998, ApJ, 497, 833
Hwang, U., Decourchelle, A., Holt, S. S., & Petre, R. 2002, ApJ, 581, 1101
Ilkov, M., & Soker, N. 2012, MNRAS, 419, 1695
Inoue, T., Yamazaki, R., Inutsuka, S.-I., & Fukui, Y. 2012, ApJ, 744, 71
Ishihara, D., Kaneda, H., Furuzawa, A., et al. 2010, A&A, 521, L61
Katsuda, S., Mori, K., Maeda, K., et al. 2015, ApJ, 808, 49
Kerzendorf, W. E., Yong, D., Schmidt, B. P., et al. 2013, ApJ, 774, 99
Khokhlov, A. M. 1991, A&A, 245, 114
Kinugasa, K., & Tsunemi, H. 1999, PASJ, 51, 239
Kothes, R., Fedotov, K., Foster, T. J., & Uyanıker, B. 2006, A&A, 457, 1081
Kozlova, A. V., & Blinnikov, S. I. 2018, J. Phys. Conf. Ser., 1038, 012006
Krause, O., Tanaka, M., Usuda, T., et al. 2008, Nature, 456, 617
Lee, S.-H., Slane, P. O., Ellison, D. C., Nagataki, S., & Patnaude, D. J. 2013, ApJ, 767, 20
Li, T. P., & Ma, Y. Q. 1983, ApJ, 272, 317
Malkov, M. A. 1999, ApJ, 511, L53
Massardi, M., López-Caniego, M., González-Nuevo, J., et al. 2009, MNRAS, 392, 733
Mattox, J. R., Bertsch, D. L., Chiang, J., et al. 1996, ApJ, 461, 396
Morlino, G., & Caprioli, D. 2012, A&A, 538, A81
Nagayoshi, T., Bamba, A., Katsuda, S., & Terada, Y. 2021, PASJ, 73, 302
Oh, K., Koss, M., Markwardt, C. B., et al. 2018, ApJS, 235, 4
Parsons, R. D., & Hinton, J. A. 2014, Astropart. Phys., 56, 26
Patnaude, D. J., Badenes, C., Park, S., & Laming, J. M. 2012, ApJ, 756, 6
Piron, F., Djannati-Atai, A., Punch, M., et al. 2001, A&A, 374, 895
Porter, T. A., Moskalenko, I. V., & Strong, A. W. 2006, ApJ, 648, L29
Prokhorov, D., Vink, J., Simoni, R., et al. 2021, Proceedings of the 37th International Cosmic Ray Conference (ICRC 2021)
Rest, A., Welch, D. L., Suntzeff, N. B., et al. 2008, ApJ, 681, L81
Reynolds, S. P. 2008, ARA&A, 46, 89
Reynolds, S. P., & Ellison, D. C. 1992, ApJ, 399, L75
Reynoso, E. M., Moffett, D. A., Goss, W. M., et al. 1997, ApJ, 491, 816
Ruiz-Lapuente, P. 2017, ApJ, 842, 112
Ruiz-Lapuente, P., Comeron, F., Méndez, J., et al. 2004, Nature, 431, 1069
Sankrit, R., Raymond, J. C., Blair, W. P., et al. 2016, ApJ, 817, 36
Slane, P., Lee, S. H., Ellison, D. C., et al. 2014, ApJ, 783, 33
Sun, L., & Chen, Y. 2019, ApJ, 872, 45
Telezhinsky, I., Dwarkadas, V. V., & Pohl, M. 2013, A&A, 552, A102
Toledo-Roy, J. C., Esquivel, A., Velázquez, P. F., & Reynoso, E. M. 2014, MNRAS, 442, 229
Totani, T., Morokuma, T., Oda, T., Doi, M., & Yasuda, N. 2008, PASJ, 60, 1327
Vink, J. 2008, ApJ, 689, 231
Vink, J. 2017, in Supernova 1604, Kepler's Supernova, and its Remnant, eds. A. W. Alsabti, & P. Murdin (Cham, Switzerland: Springer International Publishing), 139
Vink, J. 2020, in Physics and Evolution of Supernova Remnants (Cham, Switzerland: Springer International Publishing), 521
Völk, H. J., Berezhko, E. G., & Ksenofontov, L. T. 2005, A&A, 433, 229
Wang, Z. R., Qu, Q. Y., & Chen, Y. 1997, A&A, 318, L59
Williams, B. J., Borkowski, K. J., Reynolds, S. P., et al. 2012, ApJ, 755, 3
Williams, B. J., Chomiuk, L., Hewitt, J. W., et al. 2016, ApJ, 823, L32
Xiang, Y., & Jiang, Z. 2021, ApJ, 908, 22
Yuan, Q., Liu, S., & Bi, X. 2012, ApJ, 761, 133
Zabalza, V. 2015, Int. Cosm. Ray Conf., 34, 922
Zhang, X., Chen, Y., Li, H., & Zhou, X. 2013, MNRAS, 429, L25
Zirakashvili, V. N., Aharonian, F. A., Yang, R., Oña-Wilhelmi, E., & Tuffs, R. J. 2014, ApJ, 785, 130

1 Dublin Institute for Advanced Studies, 31 Fitzwilliam Place, Dublin 2, Ireland
2 Max-Planck-Institut für Kernphysik, PO Box 103980, 69029 Heidelberg, Germany
3 High Energy Astrophysics Laboratory, RAU, 123 Hovsep Emin St, Yerevan 0051, Armenia
4 Landessternwarte, Universität Heidelberg, Königstuhl 69117, Heidelberg, Germany
5 Aix Marseille Université, CNRS/IN2P3, CPPM, Marseille, France
6 Laboratoire Leprince-Ringuet, Ècole Polytechnique, CNRS, Institut Polytechnique de Paris, 91128 Palaiseau, France
7 University of Namibia, Department of Physics, Private Bag 13301, Windhoek 10005, Namibia
8 Centre for Space Research, North-West University, Potchefstroom 2520, South Africa
9 DESY, 15738 Zeuthen, Germany
10 School of Physics, University of the Witwatersrand, 1 Jan Smuts Avenue, Braamfontein, Johannesburg 2050, South Africa
11 Université de Paris, CNRS, Astroparticule et Cosmologie, 75013 Paris, France
12 Department of Physics and Electrical Engineering, Linnaeus University, 351 95 Växjö, Sweden
13 Laboratoire Univers et Théories, Observatoire de Paris, Université PSL, CNRS, Université de Paris, 92190 Meudon, France
14 Sorbonne Université, Université Paris Diderot, Sorbonne Paris Cité, CNRS/IN2P3, Laboratoire de Physique Nucléaire et de Hautes Energies, LPNHE, 4 Place Jussieu, 75252 Paris, France

[15] Université Savoie Mont Blanc, CNRS, Laboratoire d'Annecy de Physique des Particules – IN2P3, 74000 Annecy, France

[16] IRFU, CEA, Université Paris-Saclay, 91191 Gif-sur-Yvette, France

[17] Astronomical Observatory, The University of Warsaw, Al. Ujazdowskie 4, 00-478 Warsaw, Poland

[18] Instytut Fizyki Jądrowej PAN, ul. Radzikowskiego 152, 31-342 Kraków, Poland

[19] University of Oxford, Department of Physics, Denys Wilkinson Building, Keble Road, Oxford OX1 3RH, UK

[20] Université Bordeaux, CNRS, LP2I Bordeaux, UMR 5797, 33170 Gradignan, France

[21] Institut für Physik und Astronomie, Universität Potsdam, Karl-Liebknecht-Strasse 24/25, 14476 Potsdam, Germany

[22] School of Physical Sciences, University of Adelaide, Adelaide 5005, Australia

[23] Friedrich-Alexander-Universität Erlangen-Nürnberg, Erlangen Centre for Astroparticle Physics, Erwin-Rommel-Str. 1, 91058 Erlangen, Germany

[24] Laboratoire Univers et Particules de Montpellier, Université Montpellier, CNRS/IN2P3, CC 72, Place Eugène Bataillon, 34095 Montpellier Cedex 5, France

[25] Institut für Astro- und Teilchenphysik, Leopold-Franzens-Universität Innsbruck, 6020 Innsbruck, Austria

[26] Universität Hamburg, Institut für Experimentalphysik, Luruper Chaussee 149, 22761 Hamburg, Germany

[27] Obserwatorium Astronomiczne, Uniwersytet Jagielloński, ul. Orla 171, 30-244 Kraków, Poland

[28] Institute of Astronomy, Faculty of Physics, Astronomy and Informatics, Nicolaus Copernicus University, Grudziadzka 5, 87-100 Torun, Poland

[29] Nicolaus Copernicus Astronomical Center, Polish Academy of Sciences, ul. Bartycka 18, 00-716 Warsaw, Poland

[30] Institut für Astronomie und Astrophysik, Universität Tübingen, Sand 1, 72076 Tübingen, Germany

[31] Institut für Physik, Humboldt-Universität zu Berlin, Newtonstr. 15, 12489 Berlin, Germany

[32] Department of Physics, University of the Free State, PO Box 339, Bloemfontein 9300, South Africa

[33] Department of Physics and Astronomy, The University of Leicester, University Road, Leicester LE1 7RH, UK

[34] GRAPPA, Anton Pannekoek Institute for Astronomy, University of Amsterdam, Science Park 904, 1098 XH Amsterdam, The Netherlands

[35] Yerevan Physics Institute, 2 Alikhanian Brothers St., 375036 Yerevan, Armenia

[36] Kavli Institute for the Physics and Mathematics of the Universe (WPI), The University of Tokyo Institutes for Advanced Study (UTIAS), The University of Tokyo, 5-1-5 Kashiwa-no-Ha, Kashiwa, Chiba 277-8583, Japan

[37] Department of Physics, Konan University, 8-9-1 Okamoto, Higashinada, Kobe, Hyogo 658-8501, Japan

[38] Department of Physics, Rikkyo University, 3-34-1 Nishi-Ikebukuro, Toshima-ku, Tokyo 171-8501, Japan

Appendix A: SNR G4.8+6.2

In this appendix, we describe the properties of a γ-ray source candidate, SNR G4.8+6.2.

SNR G4.8+6.2 is located approximately 40 arcmin away from Kepler's SNR. The physical properties of SNR G4.8+6.2 are not well known. In the radio band, this SNR has a shell-like morphology and an angular extent of 18′ at 1.4 GHz (the NRAO VLA Sky Survey). At 2.3 GHz it appears highly polarized with an almost constant orientation of the polarization vectors across the source and with the mean fraction of polarized emission of up to 25% (Duncan et al. 1997). Young SNRs, such as Kepler's SNR, have a much smaller fractional polarization.

Appendix B: Tycho's and Kepler's SNRs

In this appendix, we describe the properties of Tycho's and Kepler's SNRs.

The distance to Tycho's SNR is estimated to be 2.5 kpc (2.5 kpc or 2.8 ± 0.4 kpc from Zhang et al. 2013; Kozlova & Blinnikov 2018, respectively), while the distance to Kepler's SNR is 5.0 ± 0.7 kpc (Ruiz-Lapuente 2017). Their measured forward shock velocities are in excess of $\sim 2000 \, \text{km s}^{-1}$ (see, for example, Hwang et al. 2002; Williams et al. 2016 for Tycho's SNR, and Vink 2008; Coffin et al. 2022 for Kepler's SNR). The downstream magnetic field strength for these SNRs are in the range of 100–200μG (Völk et al. 2005; Helder et al. 2012). The observed expansion rates of both Tycho's and Kepler's SNRs indicate that these SNRs are still in transition from the early expansion phase to the Sedov phase (Reynoso et al. 1997; Hughes 2000; Vink 2008). The X-ray spectra of both these SNRs with the presence of large amounts of iron (e.g., Hwang et al. 1998; Kinugasa & Tsunemi 1999) show that they are almost certainly of type Ia, and their classification is proven by the spectrum of a scattered-light echo from Tycho's SN (Krause et al. 2008; Rest et al. 2008) and supported by the location of Kepler SNR well above the Galactic plane, respectively. Tycho's SNR, located at a Galactic latitude of 1°4, is probably interacting with a semi-closed large molecular shell surrounding the SNR from the north to the east (Ishihara et al. 2010; Zhang et al. 2013), while Kepler's SNR, located in a lower density medium, has a density gradient with densities in the north greater by an order of magnitude than those in the south (Williams et al. 2012). The centroid position of the γ-ray emission from Tycho's SNR is consistent with the center of the shell rather than offset toward the northeastern region (Archambault et al. 2017). For both Tycho's and Kepler's SNe a single degenerate channel seems likely, given the presence of dense circumstellar gas with which the shock waves are interacting. For Kepler's SNR this is even more remarkable given its height above the Galactic plane, making a chance coincidence highly unlikely. Inside Tycho's SNR, a possible surviving companion star, known as Tycho-G, has been identified (Ruiz-Lapuente et al. 2004; Bedin et al. 2014), although the identification has been disputed (Kerzendorf et al. 2013). Inside Kepler's SNR no surviving donor star has been found, which is difficult to reconcile with a single degenerate channel, but could perhaps suggest that the donor star evolved into a (proto) white dwarf not long before the explosion. This is the so-called core-degenerate channel (Ilkov & Soker 2012; Vink 2017). The delayed-detonation model for Type Ia SNe (Khokhlov 1991) is the most probable explosion mechanism for both Tycho's and Kepler's SNe (e.g., Badenes et al. 2003; Sun & Chen 2019), resulting in the explosion energy of $E_{\text{SN}} = (1.3 - 1.6) \times 10^{51}$ erg (Gamezo et al. 2005). The light curves of Tycho's and Kepler's SNe suggest that these events are SNe Ia with the normal rate of decline after maximum light (Ruiz-Lapuente et al. 2004; Vink 2017; Ruiz-Lapuente 2017), but not slowly declining, overluminous SNe Ia (such as SN 1991T) or fast declining, underluminous SNe Ia (such as SN 1991bg). On the other hand, X-ray line intensity ratios of iron-group elements to intermediate-mass elements for Kepler's SNR are much higher than that for Tycho's SNR and correspond better to an overluminous event (Katsuda et al. 2015), and the amount of iron emission in the X-ray spectrum of Kepler's SNR rules out the subenergetic models (Patnaude et al. 2012).